Mutation Research 744 (2012) 125–134

Contents lists available at SciVerse ScienceDirect

Mutation Research/Genetic Toxicology and Environmental Mutagenesis

journal homepage: www.elsevier.com/locate/gentox
Community address: www.elsevier.com/locate/mutres

# Cytotoxic and necrotic responses in human amniotic epithelial (WISH) cells exposed to organophosphate insecticide phorate

Quaiser Saquib[a], Javed Musarrat[a,b,*], Maqsood A. Siddiqui[a], Sansa Dutta[c], Swagata Dasgupta[c], John P. Giesy[a,d,e], Abdulaziz A. Al-Khedhairy[a]

[a] Department of Zoology, College of Science, King Saud University, Riyadh, Saudi Arabia
[b] Department of Microbiology, Faculty of Agricultural Sciences, AMU, Aligarh, India
[c] Department of Chemistry, Indian Institute of Technology, Kharagpur, 721302, India
[d] Department of Biomedical and Veterinary Biosciences and Toxicology Centre, University of Saskatchewan, Saskatoon, S7 N 5B3, Canada
[e] Zoology Department and Centre for Integrative Toxicology, Michigan State University, East Lansing 48824, USA

ARTICLE INFO

*Article history:*
Received 15 September 2011
Received in revised form 7 December 2011
Accepted 7 January 2012
Available online 28 January 2012

*Keywords:*
Phorate
Cytotoxicity
Necrosis
Cell cycle
Membrane
ROS

ABSTRACT

The in vitro interaction of the organophosphorous insecticide (OPs) phorate with calf thymus DNA (ctDNA), and its potential to cause changes in cell cycle, membrane damage, and cytotoxicity leading to cell death (necrosis) was investigated in human amnion epithelial (WISH) cells. Fluorescence quenching revealed high binding affinity ($K_a = 5.62 \times 10^4\ M^{-1}$) of phorate to ctDNA. Molecular modeling of the phorate–ctDNA interaction suggested the binding of phorate at AT rich regions on minor groove of DNA. The interaction ensued alkylation of the N-6, N-7 of adenine and C-4 carbonyl oxygen of thymine. Binding of phorate was stronger in the presence of the transition metal ion copper II ($Cu^{2+}$), and has accentuated the destabilization of the DNA secondary structure. A discernable change in the voltammetric $E_{1/2}$ ($E^{0'}$) with lesser cathodic ($i_{pc}$) and anodic ($i_{pa}$) peak currents confirmed the formation of phorate–DNA and phorate–DNA–Cu (II) association complexes. Furthermore, the MTT and NRU assays demonstrated substantial phorate cytotoxicity due to loss of mitochondrial and lysosomal membrane integrity, and reduction in mitochondrial membrane potential ($\Delta\Psi m$) of treated WISH cells. Cell cycle analysis of WISH cells treated with 1000 μM phorate exhibited 13.7-fold ($p < 0.01$) augmentation in the sub-$G_1$ peak. Annexin V-PE and 7-ADD staining of phorate treated cells reaffirmed the development of late apoptotic or necrotic cell population in a concentration dependent manner. Thus, this study demonstrated the phorate induced DNA structural alterations and cellular damage in cultured human cells.



## 1. Introduction

Phorate [O,O-diethyl-S-[(ethylthio) methyl] phosphorodithioate] is a systemic organophosphorus (OPs) insecticide used to control sucking and chewing pests in pine forests and on root and field crops, including corn, cotton, coffee, and some ornamental plants and bulbs [1]. OPs exhibit the broad-spectrum activity and may pose serious health hazards when used excessively or indiscriminately [2]. OPs are esters and thioesters of phosphoric acid and thiophosphoric acid. They inhibit acetylcholinesterase activity [3] and therefore, their primary mechanism of action is neurotoxicity. Acute exposure to OPs can lead to respiratory failure, whereas chronic sub-lethal exposures can cause chronic fatigue syndrome, multiple chemical sensitivity and changes in personality [4]. When occupationally exposed to phorate, humans exhibited lesser acetylcholinesterase activity in both blood plasma and brain [5]. The United States Environmental Protection Agency (USEPA) has authorized restrictions on the use of phorate since 1990 [6]. However, it is still being used in other countries like Italy, China, Egypt and India [7–11].

Earlier studies on genotoxicity of phorate have demonstrated cytogenetic changes such as sister chromatic exchange (SCE), chromosomal aberrations (CA) and formation of micronucleus (MN) in human lymphoid and Chinese hamster ovary cells [12–14]. Recently, Mohanty et al. [15] have also reported tissue specific DNA strand breaks in rohu (*Labeo rohita*) fingerlings exposed to different concentrations of phorate. Moreover, several insecticides such as heptachlor, endosulfan, azinphos methyl, and imidacloprid exhibited the tendency to interact with DNA, and form promutagenic DNA adducts [16–18]. Also, the insecticides carbofuran and diazinon have been reported to form adducts with DNA [19,20]. All such insecticides, which either covalently bind to or intercalate into

* Corresponding author at: Al-Jeraisy Chair for DNA Research, Department of Zoology, College of Science, P.O. Box 2455, King Saud University, Riyadh 11451, Saudi Arabia. Tel.: +966 4675768; fax: +966 4675514.
*E-mail address:* musarratj1@yahoo.com (J. Musarrat).

1383-5718/$ – see front matter © 2012 Elsevier B.V. All rights reserved.
doi:10.1016/j.mrgentox.2012.01.001

DNA or form DNA adducts, can lead to gene mutations and initiate carcinogenesis, if the adducts are not repaired or are misrepaired before replication of DNA [21,22]. We have recently reported the preferential binding of phorate with tryptophan within the subdomain IIA of human serum albumin and induced protein damage [23]. However, there is no information on toxic effects of phorate on human amniotic epithelial (WISH) cells, reported in the literature. Therefore, this study has been initiated to test the hypothesis that interaction of a neurotoxic insecticide like phorate with proliferating human amniotic cells in culture may adversely affect the integrity of genetic material and exerts cytotoxic effects on exposed cells. With this aim, we have investigated the nature of interactions of phorate with DNA, especially the effects on its secondary structure and its implications on cell cycle progression. Sensitive techniques, such as fluorescence spectroscopy, circular dichroism, cyclic voltammetry and flow cytometry were applied to determine the binding of phorate to DNA and the consequent damage. Specifically, the study upon which we report here, determined: (i) binding affinity and stoichiometry of DNA–phorate complexation; (ii) the probable site of phorate binding to DNA; (iii) the role of transition metal ion Cu (II) in forming the phorate–Cu (II)–ctDNA ternary complex; (iv) the extent of induced cytotoxicity; (v) the effect of phorate on cell proliferation and perturbations in the cell cycle; and (vi) the plausible mechanism of phorate binding with accessible nitrogenous bases, as an initiation event in the process of phorate induced cytotoxicity.

## 2. Materials and methods

### 2.1. Chemicals

Calf thymus DNA (ctDNA), ethidium bromide (EtBr), propidium iodide, culture grade dimethyl sulfoxide (DMSO), $Na_2$-EDTA, Tris [hydroxymethyl] aminomethane, neutral red, RNAse, 2′,7′-dichlorofluorescin diacetate (DCFH-DA) and rhodamine dye (Rh123) were purchased from Sigma Chemical Company (St. Louis, MO, USA). RPMI-1640, L-glutamine, antibiotic–antimycotic solution, MTT (3-(4,5-dimethylthiazol-2-yl)-2,5-diphenyltetrazolium bromide and phosphate buffered saline (PBS, $Ca^{2+}$, $Mg^{2+}$ free) were obtained from Hi-Media Pvt. Ltd., Mumbai, India. Fetal bovine serum (FBS) was procured from BRL Life Technologies Inc. (Gaithersburg, MD, USA). Labware and plastic consumables were procured from Nunc A/S, Roskilde, Denmark. The ctDNA was precipitated in ethanol and dissolved in Tris–EDTA buffer pH 7.5. Purity of ctDNA was determined by measuring absorption at 260 and 280 nm. The 260/280 ratio of 1.86 indicated that the ctDNA was sufficiently free of protein. Concentrations of ctDNA were determined by use of an extinction coefficient of 6600 $M^{-1}$ $cm^{-1}$ at 260 nm. Phorate 94.6% pure was obtained from Agrochemical Division, Indian Agriculture Research Institute (IARI, New Delhi, India). Ultrapure water was used in all experiments.

### 2.2. Quantification of phorate binding to DNA by fluorescence spectroscopy

Binding of phorate to DNA was determined by use of fluorescence spectroscopy. Quenching of fluorescence was done by titration to increase the molar ratio of ctDNA to phorate. Briefly, to a fixed concentration of phorate (50 μM), increasing concentrations of ctDNA (2.5–25 μM) were added to obtain ctDNA to phorate molar ratios from 0.05 to 0.5 in 10 mM Tris–HCl buffer at ambient temperature. Spectra were recorded under subdued light to prevent undesired photodegradation. Fluorescence was determined by use of a Shimadzu spectrofluorophotometer, model RF5301PC equipped with RF 530XPC instrument control software, Kyoto (Japan). The path length was 1 cm in a quartz cell. Excitation and emission slits were set at 3 and 10 nm, respectively. The excitation and emission wavelengths were 246 nm and 272 nm, respectively. ctDNA alone does not fluoresce at this wavelength. The fluorescence quenching constant was determined by use of the Stern–Volmer relationship (Eq. (1)) as described previously [22].

$$\frac{F_0}{F} = 1 + \mathrm{Ksv}[Q] \quad (1)$$

where $F_0$ and $F$ are the fluorescence intensities in the absence and presence of the quencher (ctDNA), respectively, Ksv is the Stern–Volmer quenching constant and [Q] the quencher concentration. The quenching constant was obtained from the slope of the Stern–Volmer plot ($F_0/F$ versus [Q]). The binding constant ($K_a$) and number of binding sites ($n$) were estimated, following previously published methods [24,25] (Eq. (2)) and assuming a 1:0.5 complex between phorate and ctDNA, as described previously [22].

$$\frac{F_0 - F}{F - F_\infty} = K_a \times [\mathrm{DNA}] \quad (2)$$

where $F_0$ and $F_\infty$ are the relative fluorescence intensities of phorate alone and phorate saturated with ctDNA, expressed as the relative fluorescence intensity of ctDNA to phorate molar ratio of 1:0.5, respectively. The slope of the linear portion of the double-logarithm plot (Log$[(F_0 - F)/(F - F_\infty)]$ versus Log[ctDNA] provided the number of equivalent binding sites ($n$). However, the value of Log[ctDNA] at Log$[(F_0 - F)/(F - F_\infty)] = 0$ is equal to the negative logarithm of the binding constant ($K_a$) [22]. Also, the influence of divalent metal ion Cu (II) on the binding of phorate–DNA was determined at a molar ratio of 1:0.2.

### 2.3. Binding of phorate–DNA determined by cyclic voltammetry

The redox potentials of phorate and the phorate–ctDNA complex in the absence and presence of Cu (II) were determined at room temperature in an aqueous medium containing 0.4 M $KNO_3$, as a supporting electrolyte, by use of an Electrochemical Analyzer, CH Instruments, Texas (USA). A conventional three-electrode system was employed with a platinum microcylinder as working electrode, platinum wire as an auxiliary electrode and Ag/AgCl as a reference electrode. The formal potential ($E^{0'}$) or half wave potential ($E_{1/2}$) was calculated from the average of the anodic ($E_{pa}$) and cathodic ($E_{pc}$) peak potentials. Peak potential separation $\Delta E_p$ was determined by subtracting cathodic ($E_{pc}$) and anodic ($E_{pa}$) peak potentials.

### 2.4. Circular dichroism (CD) measurements

CD spectra of phorate were used to determine the change in optical behavior of phorate in the presence and absence of ctDNA. CD measurements of phorate alone (20 μM) and in the presence of 50 and 100 μM of ctDNA were obtained in 1 cm path length cell on Jasco model J-815, spectro-polarimeter, Tokyo (Japan), calibrated with d-10-camphorsulphonic acid. CD measurements were conducted at 25 °C with a thermostatically controlled cell holder attached to a NESLAB RTE-110 circulating water bath (NESLAB Instruments Inc., New Hampshire, USA), with an accuracy of ±0.1 °C. Spectra were collected at a scan rate of 100 nm/min with a response time of 1 s. Each spectrum was the average of four scans and corrected by subtraction of a buffered blank under identical conditions with results expressed as CD [mdeg].

### 2.5. Docking analysis of phorate–DNA interaction

The B-DNA crystal structure used for the docking studies was obtained from the Protein Data Bank with identifier 453D [26]. The DNA file was prepared for docking by removing water molecules and adding polar hydrogen atoms with Gasteiger charges. The 3D structure of the ligand (phorate) was generated in Sybyl 6.92 (Tripos Inc., St. Louis, USA) and its energy-minimized conformation was obtained by use of the MMFF94 force field represented by MMFF94 charges. The rotatable bonds in the ligand were assigned by use of AutoDockTools and docking was conducted by use of AutoDock 4.0 Lamarckian Genetic Algorithm (GA) [27,28]. DNA was enclosed in a grid having 0.375–0.431 Å spacing. Other miscellaneous parameters were assigned the default values given by AutoDock. The output from AutoDock was rendered in PyMol [29].

### 2.6. Cell culture

Cytotoxicity of phorate to human epithelial amnion (WISH) cells was assessed by flow cytometry. Amnion derived WISH cells (American Type Culture Collection (CCL-25), Rockville, MD, USA) are being maintained in our laboratory at King Saud University, Riyadh. The diploid WISH cells exhibiting growth with no contact inhibition were grown in RPMI-1640 supplemented with 10% FBS and antibiotic–antimycotic solution (100×, 1 ml/100 ml of medium) at 37 °C in a 5% $CO_2$ atmosphere with 95% humidity. Cell viability was assessed by visual microscopic inspection for exclusion of trypan blue. Batches of WISH cells exhibiting less than 95% cell viability were not used. Since, no significant effects were observed at durations of 24 or 48 h, the duration of exposure to phorate was 72 h, unless otherwise specified.

### 2.7. Tetrazolium bromide salt (MTT) assay

Viability of phorate-treated WISH cells was assessed by use of the MTT assay, as described previously [30]. In brief, cells ($1 \times 10^4$) were allowed to adhere for 24 h in 96-well plates, and then exposed to concentrations of phorate ranging from 1 to 1000 μM. Subsequently, 10 μl of 5 mg MTT/ml stock in PBS was added to each well and incubated at 37 °C for 4 h, after which the medium was removed and 200 μl of DMSO added to each well and mixed gently. The plate was then kept on a rocker shaker for 10 min at room temperature and the purple color developed was read at 550 nm by use of a multi-well microplate reader (Biochrom Anthos Zenyth 200, Cambridge, UK). The solvent control (0.1% DMSO) was also run under identical conditions.

### 2.8. Neutral red uptake (NRU) assay

The neutral red uptake (NRU) assay was used to measure cell viability. The NRU assay was conducted following the protocol described previously [31]. Briefly, cells were exposed to phorate concentrations of 1–1000 μM. Medium was removed after 72 h and cells were washed twice with PBS, and incubated for 3 h in medium supplemented with neutral red (50 μg/ml). Medium was washed off rapidly with a solution containing 0.5% formaldehyde and 1% calcium chloride. To extract the dye, cells were incubated for 20 min at 37 °C in a mixture of acetic acid (1%) and ethanol (50%) and absorbance measured at 540 nm. Values were compared with solvent control (0.1% DMSO) where the NRU assay was conducted under identical conditions.

### 2.9. Mitochondrial membrane potential

Mitochondrial membrane potential was determined following the method as described previously [32]. In brief, the solvent control (0.1% DMSO) cells and those treated with 500 or 1000 μM phorate for 72 h were harvested and centrifuged at 3000 rpm for 5 min. Pellets of cells were washed twice with cold PBS and resuspended in 500 μl of PBS. Cells were further incubated with rhodamine (Rh123) (5 μg/ml) for 60 min at 37 °C in dark with gentle shaking. The greater concentrations were chosen since no significant effects were observed at phorate concentrations less than 250 μM. The membrane potential was calculated as the mean fluorescence intensity (Log FL1 488 nm) of 10,000 cells. Mitochondrial activity was also monitored by observing changes in fluorescence intensity of the mitochondria-specific dye (Rh123) in WISH cells, as described previously [32]. The solvent control (0.1% DMSO) cells and those treated with 50, 100, 250, 500 or 1000 μM phorate for 72 h at 37 °C were stained with 20 μM Rh123 for 1 h at 37 °C, and visualized under a fluorescence microscope (Nikon, Eclipse E600, Tokyo, Japan) at excitation and emission wavelengths of 520 and 590 nm, respectively.

### 2.10. TEM analysis of WISH cells

Changes in ultrastructure in the phorate treated cultured WISH cells were studied with transmission electron microscopy (TEM) using the method as described previously [32]. In brief, the cells were exposed to 500 and 1000 μM phorate for 72 h at 37 °C. Subsequently, the ultrathin sections of glutaraldehyde fixed untreated and phorate treated cells, embedded in low viscosity araldite resin were prepared, and visualized under high vacuum at 100 kV using JEOI-1011 Electron Microscope (JEOL, Tokyo, Japan).

### 2.11. Intracellular ROS generation

Phorate-induced generation of reactive oxygen species (ROS) in WISH cells was observed using a fluorescent probe DCFH-DA following the method described previously [32]. Briefly, WISH cells were cultured for 72 h in the presence of 50, 100, 250, 500 or 1000 μM phorate at 37 °C in 5% $CO_2$ atmosphere. Cells were washed 3 times with cold PBS and stained with 5 μM of DCFH-DA for 1 h at 37 °C. The solvent control (0.1% DMSO) and phorate-treated WISH cells were visualized by use of a fluorescence microscope (Nikon, Eclipse E600) at the excitation and emission wavelengths of 485 and 530 nm, respectively.

### 2.12. Flow cytometric analysis of cell cycle progression and apoptosis/necrosis

WISH cells treated with 0.1% DMSO as a solvent control or cells treated with 50–1000 μM phorate for 72 h were harvested and centrifuged at 1000 rpm for 4 min. Pellets were resuspended in 500 μl of PBS. Cells were fixed with equal volume of chilled 70% ice-cold ethanol, and incubated at 4 °C for 1 h. After two successive washes with PBS at 1000 rpm for 4 min, cell pellets were resuspended in PBS and stained with 50 μg propidium iodide (PI)/ml containing 0.1% Triton X-100 and 0.5 mg/ml RNAase A for 1 h at 30 °C in dark. Fluorescence of the PI was measured by flow cytometry by use of a Beckman Coulter flow cytometer (Coulter Epics XL/Xl-MCL, Miami, USA) through a FL-4 filter (585 nm) and 10,000 events were acquired [33]. The data were analyzed by Coulter Epics XL/XL-MCL, System II Software, Version 3.0. Cell debris was characterized by a low FSC/SSC was excluded from the analysis.

### 2.13. Evaluation of apoptosis/necrosis with annexin V-PE and 7-AAD

Apoptosis and/or necrosis in phorate treated WISH cells were investigated by flow cytometry by use of the two-color variation of phycoerythrin-labeled annexin V (annexin V-PE) and cell viability dye 7-amino-actinomycin D (7-AAD) (Cell Lab ApoScreen™ Annexin V-PE Apoptosis Kit, Cat No. 736518, Beckman Coulter, USA). Positioning of quadrants along the axes of annexin V-PE vs. 7-AAD was used to display the relationships between the number of live cells (annexin $V^-$/7-$AAD^-$), early apoptotic cells (annexin $V^+$/7-$AAD^-$), late apoptotic cells (annexin $V^+$/7-$AAD^+$) and necrotic cells (annexin $V^-$/7-$AAD^+$) [34]. WISH cells were exposed to 50, 100, 250, 500 or 1000 μM phorate for 72 h at 37 °C with 5% $CO_2$, and the harvested cells were processed further as per manufacturer's protocol. In brief, the cell suspension was washed twice with cold PBS and the cell pellets were resuspended to a concentration of $1 \times 10^6$ cells/ml in cold 1× binding buffer. An aliquot of 100 μl of cell suspension from each treatment was incubated with 10 μl of annexin V-PE for 15 min in dark on ice followed by the addition of 10 μl of 7-AAD and 380 μl of cold 1× binding buffer to each tube and analyzed within 30 min after staining. The fluorescence of 10,000 cells was recorded by use of a 488 nm excitation wavelength and the fluorescence of annexin V-PE and 7-AAD were expressed on a log scale after enumeration through FL1 filter (525 nm) and FL-2 filter (570 nm) on the Beckman Coulter flow cytometer (Coulter Epics XL/Xl-MCL, USA).

### 2.14. Statistical analyses

Data were expressed as mean ± S.D. for the values obtained from at least three independent experiments. Statistical analysis was performed by one-way analysis of variance (ANOVA) using Dunnett's multiple comparisons test (Sigma Plot 11.0, USA). The level of statistical significance chosen was $^*p < 0.05$, unless otherwise stated.

## 3. Results

### 3.1. Fluorescence quench titration of phorate upon binding with ctDNA

The intrinsic fluorescence of phorate was inversely proportional to ctDNA to phorate molar ratios when fluorescence emission spectra of phorate and phorate–ctDNA complex were measured at an excitation wavelength of 246 nm (Fig. 1A). Maximum quenching of fluorescence of 40.7% was observed at the greatest ctDNA to phorate molar ratio of 1:0.5. The quenching constant (Ksv) derived from the plot of $F_0/F$ versus [Phorate] × $10^6$ M (Fig. 1B) and Stern–Volmer algorithm was $2.78 \times 10^4\ M^{-1}$ ($r^2 = 0.99$). The binding constant ($K_a$), determined from the fluorescence data plotted as $\log[(F_0 - F)/(F - F_\infty)]$ versus log[ctDNA]) (Supplement Fig. 1A) was $5.62 \times 10^4\ M^{-1}$ and the number of binding sites ($n$) was 1.13. When $K_a$ was estimated by use of the modified Stern–Volmer plot a similar value was obtained ($4.12 \times 10^4\ M^{-1}$, $r^2 = 0.99$) (Supplement Fig. 1B). The free energy ($\Delta G$), entropy ($\Delta S$) and enthalpy ($\Delta H$) changes for the formation of the phorate–ctDNA complex were −6.357 kcal/mole, 0.1819 J/mole and 6.38 kcal/mole, respectively. Furthermore, the effect of transition metal ion Cu (II) on phorate–ctDNA binding is shown in Supplement Fig. 2. The presence of 10 μM of transition metal ion Cu (II) on phorate–ctDNA binding at a phorate–Cu (II) molar ratio of 1:0.2 resulted in 13.4% decline in the fluorescence intensity of phorate alone. However, the reduction in intrinsic fluorescence of phorate in combination with ctDNA alone and phorate–ctDNA–Cu (II) complex were 53.48% and 57.52%, respectively. The results exhibit more fluorescence quenching with ctDNA–Cu (II) than ctDNA or Cu (II) alone. Thus, the fluorescence studies suggest high phorate–ctDNA binding affinity and formation of a phorate–ctDNA–Cu (II) tertiary complex in the presence of Cu (II) ions.

### 3.2. Voltammetric analysis of phorate–DNA binding

In the range of +0.2 V to −1.2 V, phorate formed complexes in the presence of DNA and Cu (II) at room temperature. The cyclic voltammogram of phorate, as a ligand, exhibits a quasi-reversible redox peak with $\Delta E_p$ value of 319 mV (Fig. 2A). Equimolar addition of DNA to phorate, changed $\Delta E_p$ values to 327 mV. However, no change in the $\Delta E_p$ was observed with the addition of Cu (II) alone. The cathodic ($i_{pc}$) and anodic ($i_{pa}$) peak currents as well as their ratio ($i_{pa}/i_{pc}$) were less in the presence of DNA. Addition of Cu (II) to the phorate–DNA complex resulted in a higher cathodic ($i_{pc}$) peak current; while the cathodic peak potential ($E_{pc}$) was shifted negatively. However, under identical conditions, at a scan rate of $0.3\ V\ s^{-1}$, the anodic peak potential ($E_{pa}$) was shifted toward a less negative value. $E^{0'}$ or $E_{1/2}$ values were −0.271 and −0.275 for phorate and phorate plus DNA. Addition of DNA to phorate solution at a 1:1 molar ratio shifted $E_{1/2}$ negatively. Overall, the phorate–DNA interactions without and with Cu (II) exhibited characteristic changes in the peak current values and redox potential indicative of complex formation.

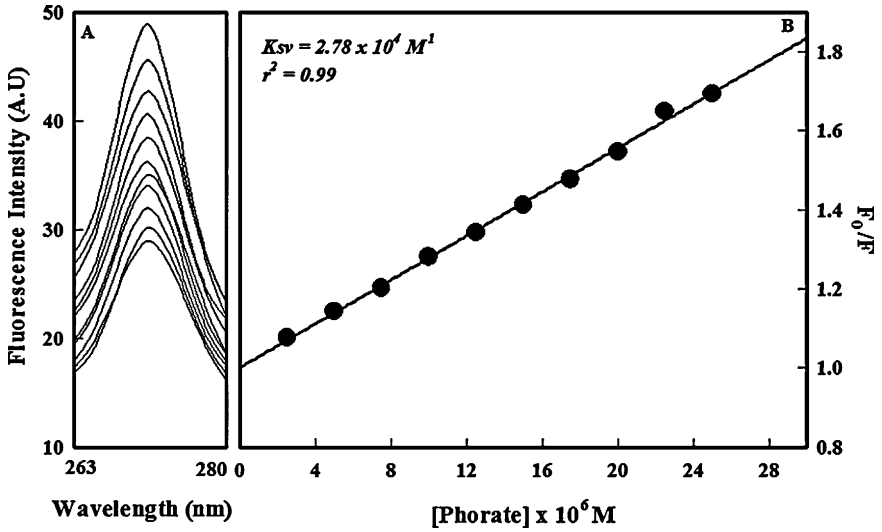


**Fig. 1.** Fluorescence quench titration of phorate with ctDNA. Panel (A) depicts fluorescence emission spectra of phorate in the absence (uppermost curve) and presence of increasing amounts of ctDNA at excitation wavelength of 246 nm. The molar ratio of ctDNA to phorate varies from 0.05 to 0.5 (top to bottom). Panel (B) represents the Stern–Volmer plot based on phorate–ctDNA fluorescence quenching data.

### 3.3. Circular dichroism of phorate–DNA complexes

The CD spectrum of the phorate interaction with DNA at molar ratios of 1:2.5 and 1:5 exhibited positive bands at 201, 207, 210, 213 and 215 nm, respectively (Fig. 2B). Addition of DNA at a molar ratio of 1:5 resulted in disappearance of the phorate parent peaks at 201, 210 and 213 nm. At the same molar ratio, the peak of phorate at 215 nm exhibited a blue shift of 7 nm with the emergence of a new peak at 214 nm. The CD data exhibited reduction in the phorate ellipticity and structural alterations in the secondary structure of DNA.

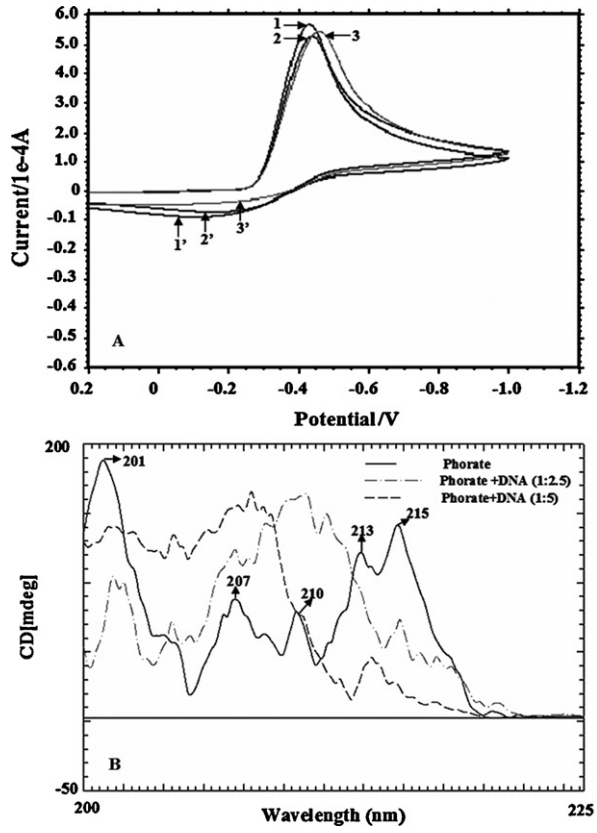


**Fig. 2.** Panel A: Cyclic voltammograms showing typical Nernstian behavior of phorate at a scan rate of 0.3 V $s^{-1}$. The peaks marked with arrows are represented as: Curve 1: phorate (1 mM); Curve 2: phorate (1 mM) + DNA (1 mM); Curve 3: phorate + DNA + Cu (II) (1 mM each). The curves 1–3 and 1′–3′ represent the oxidation and reduction peaks, respectively. Panel B: CD analysis of phorate–DNA binding. The spectra were recorded with phorate (20 μM) in 10 mM in Tris–HCl buffer, pH 7.4 in the absence and presence of 50 and 100 μM DNA. The characteristic positive bands of phorate are indicated with arrows.

### 3.4. Molecular modeling of phorate–DNA interaction

The docked structure revealed that phorate fits within the minor groove of DNA encompassing a length corresponding to ~3 base pairs (Fig. 3A). The distance of the ligand from the O-4 of thymine (T) and N-6 and N-7 of adenine (A) is a characteristic feature of chemicals that bind in the minor groove. The change in accessible surface area for interacting with residue A18 also indicates preferential binding of phorate to the AT regions of ctDNA. The change in accessible surface area and distance of DNA nucleo-bases as a consequence of phorate binding to DNA are given in Fig. 3B. The free energy of binding ($\Delta G$), estimated by the docking analysis was −10.93 kcal/mol, which is slightly greater than the free energy of −6.357 kcal/mole that was determined experimentally.

### 3.5. Phorate induced cytotoxicity in WISH cells

Exposure of WISH cells to phorate for 72 h resulted in significant cytotoxicity with a concentration dependent decrease in survival of cells. Based on the results of the MTT assay, exposure of WISH cells to 1, 10, 100, 250, 500 or 1000 μM phorate, resulted in 6.0%, 9.2%, 12.2%, 18.0%, 27.3% and 63.4% reduction in cell viability relative to that of the solvent control (Fig. 4A). Similarly, based on the results of the NRU assay also demonstrated cytotoxicity of phorate, but there was a relatively less survival of cells exposed to concentrations of 100 μM or greater (Fig. 4B). The percent reduction in cell viability at concentrations of 250, 500 or 1000 μM phorate relative to the solvent controls were 22.0, 72.0 and 83.2%, respectively. The greatest concentration of phorate (1000 μM) causing 63.6 and 83.2% decline in cell viability based on the results of the MTT and NRU assays, respectively.

A

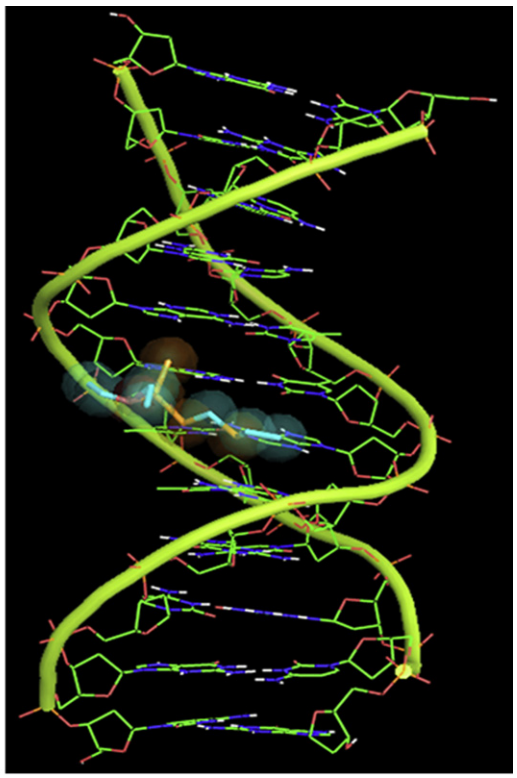

B

| Nucleobases | Distance (Å) |
|---|---|
| A-5 (N7) | 2.70 (9-S) |
| A-6 (N6, N7) | 3.05, 3.34 (9-S) |
| T-7 (O4) | 3.43 (5-S) (10.01)* |
| A-17 (N7) | 2.70 (11-S) |
| A-18 (N6, N7) | 2.77 (5-S), 3.25 (11-S) (18.34)* |

**Fig. 3.** Panel A: Representing the docking pose of energy-minimized structure of phorate–ctDNA complex. Panel B: shows the distances (Å) of nucleobases from phorate in ctDNA–phorate complex. (*) Values in the parenthesis represent the accessible surface area (ΔASA) in Å$^2$.

### 3.6. Effect of phorate on mitochondrial membrane potential and ROS generation

The Log FL1 peak of the Rh123 probe in the flow cytometry data was shifted to the left, when WISH cells were treated with 500 or 1000 μM phorate, as compared to the solvent control (Fig. 5, Panel IA). This represents a significant decrease in mitochondrial membrane potential ($\Delta\Psi m$) of 12.5% and 38.6% in WISH cells exposed to 500 and 1000 μM phorate for 72 h, respectively. Since no significant decline and/or shift was observed in the spectra at the lesser concentrations of 50, 100 or 250 μM phorate, only spectra from the two greatest concentrations are shown (Fig. 5, Panel IB).

The TEM images of effects of phorate on the ultrastructure of treated cells are shown in Fig. 5, panel II. The results clearly indicate disappearance of mitochondrial cristae at 500 μM and necrosis at 1000 μM phorate. Cells treated with 500 μM phorate also

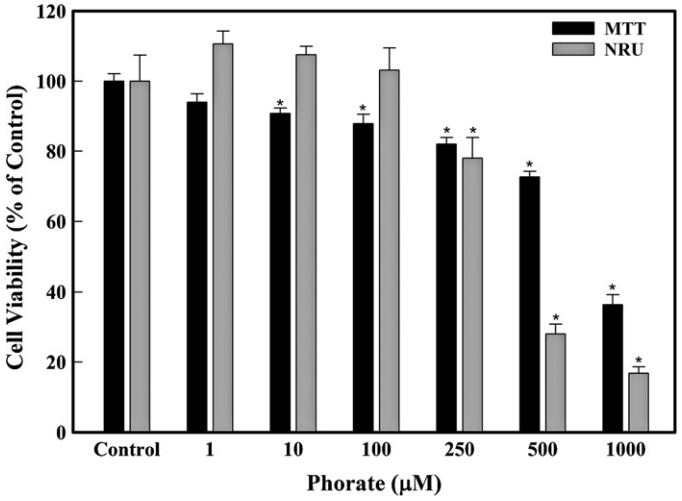


**Fig. 4.** Cytotoxicity assessment of phorate in human amnion epithelial (WISH) cells showing the percent cell viability after 72 h of phorate exposure using MTT and NRU assays, respectively. Each histogram represents the mean ± S.D. values obtained from three independent experiments. *$p < 0.05$ vs. control.

exhibited the disappearance of nucleolus, nuclear condensation and membrane blebbing. Changes in mitochondrial membranes of phorate-treated WISH cells were further validated by observing alterations in mitochondrial activity under fluorescence microscopic of the cationic fluorescent probe Rh123, which is strongly accumulated electrophoretically by the negatively charged matrix of mitochondria in control cells. Accumulation is inversely proportional to phorate concentration (Fig. 6 panel I). Exposure to 50–250 μM phorate also caused blebbing of cell membranes and significantly fewer cells at 500 or 1000 μM phorate.

Intracellular ROS were assessed based on detection of peroxide-dependent oxidation of DCFH-DA to fluorescent 2′,7′-dichlorofluorescin (DCF). Up to a concentration of 250 μM increase in the fluorescence of DCF was directly proportional to phorate concentration and comparatively greater than that of the solvent control (0.1% DMSO) cells (Fig. 6 panel II). However, due to significant cell death (necrosis) the DCF fluorescence intensity was less at 500 or 1000 μM phorate (Fig. 6 panel II).

### 3.7. Phorate induced cell death (late apoptosis/necrosis) in WISH cells

Cell cycle analysis of PI-stained solvent control and phorate treated cells indicates an increase in sub-$G_1$ peak with concomitant reduction in $G_1$ and $G_2$/M phases (Fig. 7A and B). A significant increase in the proportions of dead cells in sub-$G_1$ phase were 15.3 ± 0.66%, 22.5 ± 1.32%, 28.3 ± 0.7%, 32.7 ± 1.1% and 54.8 ± 3.3% in populations of WISH cells exposed to 50, 100, 250, 500 or 1000 μM phorate, respectively. The proportion of dead cells in the solvent control population was 3.98 ± 0.08%. Significantly low percent of cells appeared in the $G_1$ and $G_2$/M peaks in WISH cells exposed to 1000 μM phorate (23.4 ± 1.6% and 19.23 ± 0.8%, $p < 0.01$), compared to 47.2 ± 0.8% and 36.9 ± 0.5%, respectively in solvent control cells. Phorate-induced cell death was further validated by use of the annexin V-PE and 7-AAD apoptotic assay. The results are represented by use of a dot plot, which represents fluorescence generated upon binding of annexin V-PE with phosphatidylserine on the plasma membrane of apoptotic/necrotic cells and exclusive staining of necrotic cells with 7-AAD (Fig. 8). Based on the annexin V-PE and 7-ADD staining, 83.8% of cells in solvent control were alive with 0.1, 2.6 and 14.5% of cells classified as being in early, late and necrotic stages. Exposure to 50, 100, 250, 500 or

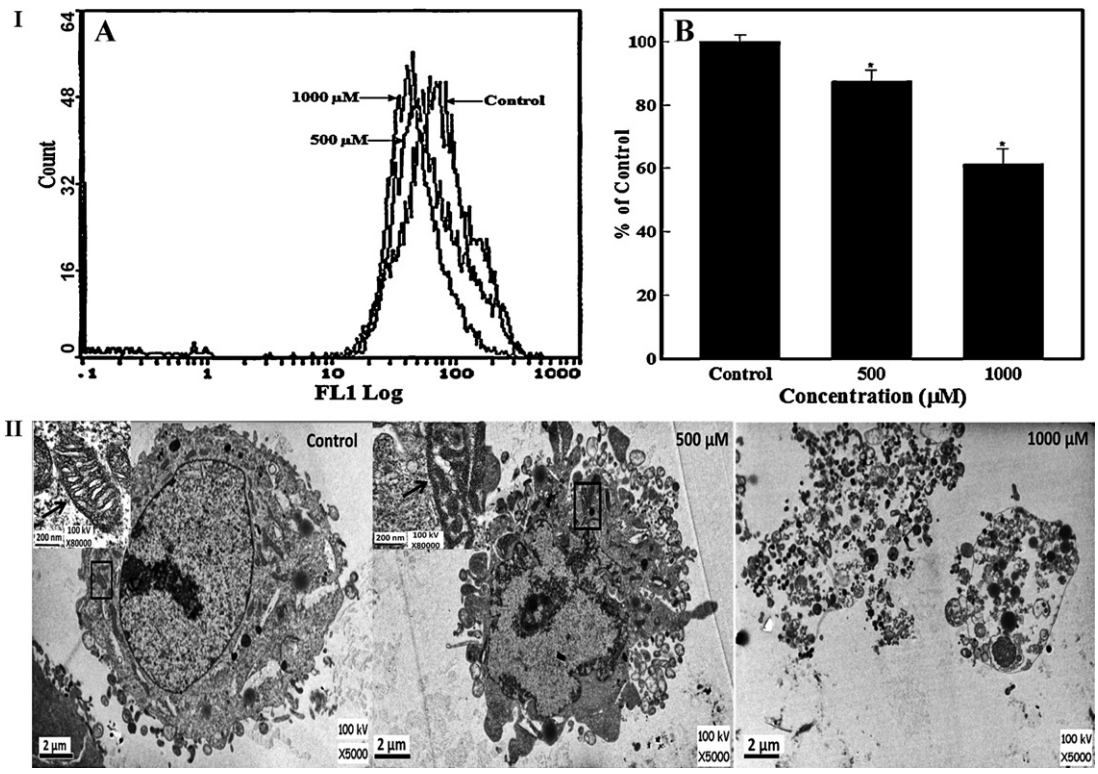


**Fig. 5.** Flow cytometric and ultrastructure analyses of phorate induced mitochondrial membrane damage. Panel I A: a representative flow cytometric spectra exhibiting reduction in mitochondrial membrane potential ($\Delta\Psi m$) in phorate treated WISH cells. Each histogram in panel I B represents mean ± S.D. values of Rh123 fluorescence obtained from three independent experiments (*$p < 0.05$ relative to control). Panel II: exhibit the representative TEM images indicating the cellular and mitochondrial changes in phorate treated WISH cells. Magnification at 5000×, shows representative mitochondria in box and the insets at magnification 80,000×, shows their enlarged images, marked with arrow in the photomicrographs.

1000 μM phorate resulted in necrosis, which is represented by a shift of 19.8, 27.2, 47.2, 53.8 and 74.3%, respectively of cells into the upper left quadrant of the annexin $V^-$/7-$AAD^+$ plot which represents necrotic cells. An increase of 3.5, 4.2 and 8.7% in the proportion of cells in the upper right quadrant of the annexin $V^+$/7-$AAD^+$ plot, which represents late apoptotic cells was caused by exposure to 250, 500 or 1000 μM phorate. Virtually, no cells fell in the lower right quadrant, which is specific for apoptosis.

## 4. Discussion

The fluorescence quenching of intrinsic fluorescence of phorate upon addition of ctDNA was most likely due to masking of phorate chromophores within the helix due to surface binding at the reactive nucleophilic sites on the heterocyclic nitrogenous bases of ctDNA molecule. The results of the fluorescence studies were consistent with electrostatic interactions of phorate with ctDNA that resulted in formation of a phorate–ctDNA binary complex. The quenching constant (Ksv) determined using the Stern–Volmer algorithm, is indicative of the affinity of this insecticide toward DNA. Typically, the linearity of the Stern–Volmer plot suggests the (i) existence of one binding site for the ligand in proximity of fluorophore, or (ii) more than one binding site equally accessible to the ligand [35]. In order to elucidate the mode of interaction, displacement of EtBr by phorate was determined. The fact that addition of phorate to the EtBr–ctDNA complex did not result in less fluorescence (data not shown) suggests the non-intercalative nature of phorate binding. Thermodynamic parameters such as the changes in free energy ($\Delta G$) due to ligand binding also provide insight into the binding mode. The negative $\Delta G$ values for the interaction of ctDNA with phorate indicate the spontaneity of the complexation. The interaction process has been found to be entropy driven and the major contribution of $\Delta G$ comes from positive $\Delta S$. The observation that both the $\Delta H$ and $\Delta S$ for phorate binding to DNA were positive is consistent with complexation of ctDNA with phorate involving hydrophobic interaction. Hydrogen bonds, van der Waals, hydrophobic and electrostatic interactions are the major interactions that play a key role in molecular recognition [36]. Addition of Cu (II) resulted in the formation of phorate–Cu (II)–ctDNA complex, which further augments the conformational changes by the local unwinding, caused loss of helical integrity of duplex DNA. The typical quasi-reversible redox peaks of cyclic voltammogram of phorate, as a small ligand, upon interaction with DNA and DNA–Cu (II) produced changes in the $\Delta E_p$ and $E^{0'}$ values. The negative shift in formal potential ($E^{0'}$) indicated that phorate binds favorably with DNA via electrostatic binding [37]. The decrease of cathodic ($i_{pc}$) and anodic ($i_{pa}$) peak currents and shift of $E^{0'}$ suggests the formation of phorate–DNA and phorate–DNA–Cu (II) complexes. The decline in peak currents may be due to the imbalance in the equilibrium concentration of free phorate in solution owing to the presence of DNA, which induces the diffusion of phorate–DNA complex, and not due to blockage of the electrode surface by an adsorbed layer of DNA that could possibly form at the electrode surface [20,38].

Because phorate is optically active and the enantiomers exhibit a CD spectrum, which can be used to validate binding of phorate with DNA. The fact that addition of ctDNA to phorate in molar ratios of 1:2.5 and 1:5 exhibited substantial change in ellipticity values suggests the formation of phorate–DNA binary complex. The results of the docking studies substantiated the phorate–ctDNA interaction. The docked structure revealed that phorate could fit within the minor groove with a binding site of three base pairs long that preferably involves A–T residues. A similar type of interaction has been reported between the fungicide (methyl thiophanate) and ctDNA

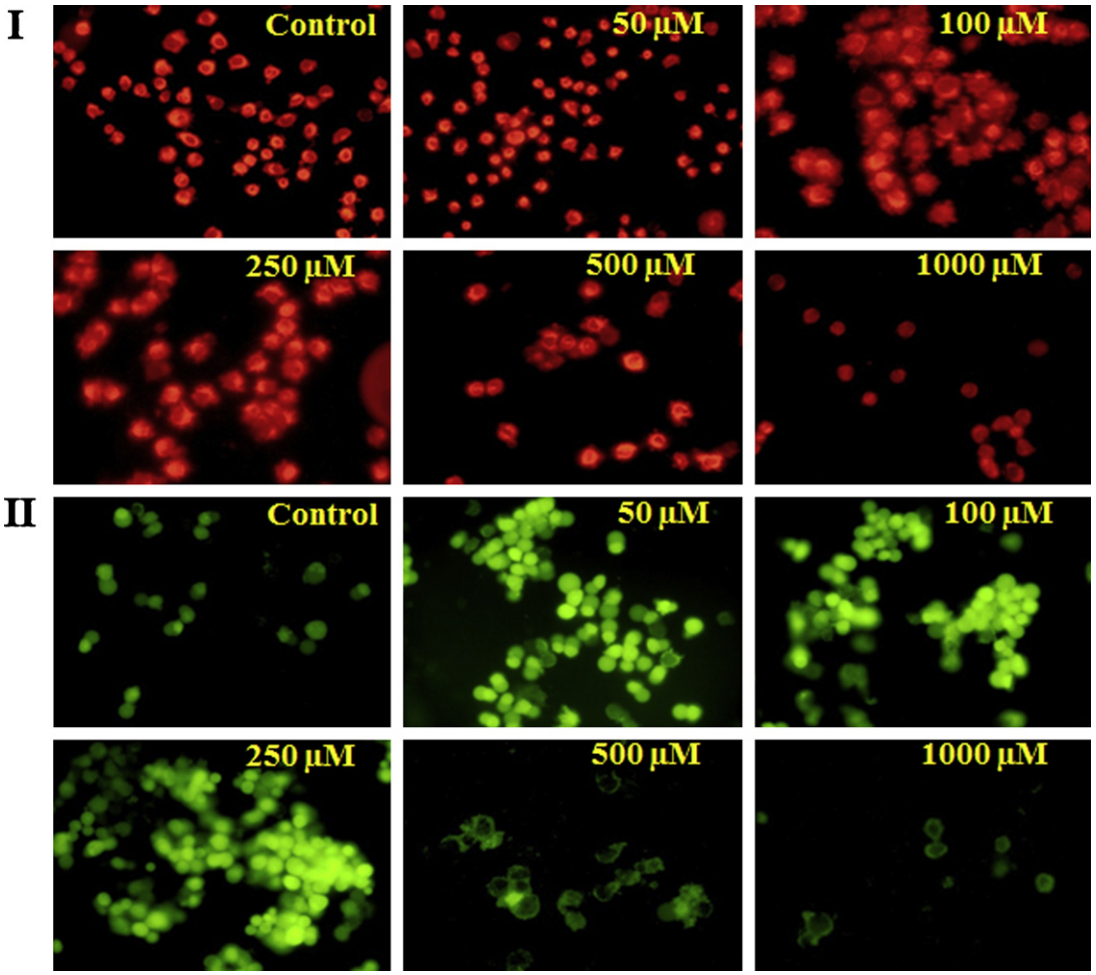


**Fig. 6.** Fluorescence analysis of the changes in mitochondrial membrane potential and intracellular ROS generation in phorate treated WISH cells. Panel I shows the reduction in the intensity of Rh123 fluorescent probe in treated cells. Panel II shows the phorate concentration dependent enhancement in green fluorescence of DCF due to ROS generation up to 250 μM. Fluorescence decrease at higher concentration of 500 and 1000 μM signifies the cell death due to necrosis.

[22]. The narrow A–T regions as compared to G–C regions provides a better fit of small molecules into the minor groove, and involves the van der Waals interactions with the DNA functional groups that define the groove. The theoretical models (Supplement Figs. 3 and 4) suggest the possibility of ethyl group ($^{+}CH_3CH_2$) transfer from phorate to AT base pairs in DNA. A likely mechanism is interaction of phorate with intracellular Cu (II), which results in the formation of stable complex and releases transient activated species. This could occur due to the transfer of a free lone pair of electrons, at neutral pH, at the reactive O-3 and O-1′ positions on the bilaterally symmetrical arms of phorate. The ethyl moieties then preferentially attack the nucleophilic centers, and possibly trapped at N-6 and N-7 of adenine (A) or C-4 carbonyl oxygen of thymine (T). The addition of ethyl group to the nitrogenous base may perturb the aromatic character, causing hydrogen bond breakage, and consequently leads to GC to AT transitions, if unrepaired. The suggested alkylation at N-6, N-7 and C-4 carbonyl oxygen positions of A and T, respectively supports our phorate–DNA binding and docking studies, and considered as an important factor in causing phorate induced toxicity and DNA damage. We have recently demonstrated significant DNA damage through comet assay, in terms of the Olive tail moment, in bone marrow cells of animals (male Wistar rats) treated at doses of 0.092 and 0.184 mg phorate/(kg bw/day) for 14 days via oral route, as compared to control [39]. Furthermore, our studies on phorate induced DNA damage in rat peripheral blood mononuclear cells (PBMNC) have also demonstrated 14.3-fold increase in DNA damage vis-à-vis vehicle control. The comet data revealed the OTM values of $0.92 \pm 0.05$ and $1.43 \pm 0.17$ ($p < 0.05$) in PBMNC of rats at phorate doses of 0.092 and 0.184 mg/(kg bw/day), respectively, compared to $0.10 \pm 0.01$ in controls (Supplement Table 1 and Supplement Fig. 5). Similarly, Mahli and Grover [40] and Dhingra et al. [14] have also shown phorate induced chromosomal aberrations (CA) and micronuclei formation (MN) in rat bone marrow cells at doses of 0.15–0.30 mg phorate/(kg bw/day) and 7.5–15 mg phorate/kg bw, respectively and supports our observations.

The MTT and NRU data revealed significant phorate cytotoxicity in cultured WISH cells as evident with the damage in mitochondrial and lysosomal membranes, eventually triggering cell death. The cytotoxic effect at the higher concentration of 250 μM was more pronounced with the NRU vis-à-vis MTT assay, which could be attributed to a greater lysosomal damage as compared to the mitochondria. Indeed, the weakly cationic, supravital NR dye penetrates the cell membranes of normal cells by non-ionic diffusion and accumulates intracellularly in lysosomes. Phorate-induced alterations in the cell surface or sensitive lysosomal membrane lead to lysosomal fragility, which resulted in decreased uptake and binding of NR. This made it possible to distinguish between viable and dead cells via spectrophotometric measurements. The concentration-dependent cell lethality measured by the MTT and NRU assays in phorate-treated cells demonstrated cytotoxicity, and served as a sensitive, integrated measure of cell integrity and inhibition of cell division. These results are consistent with the

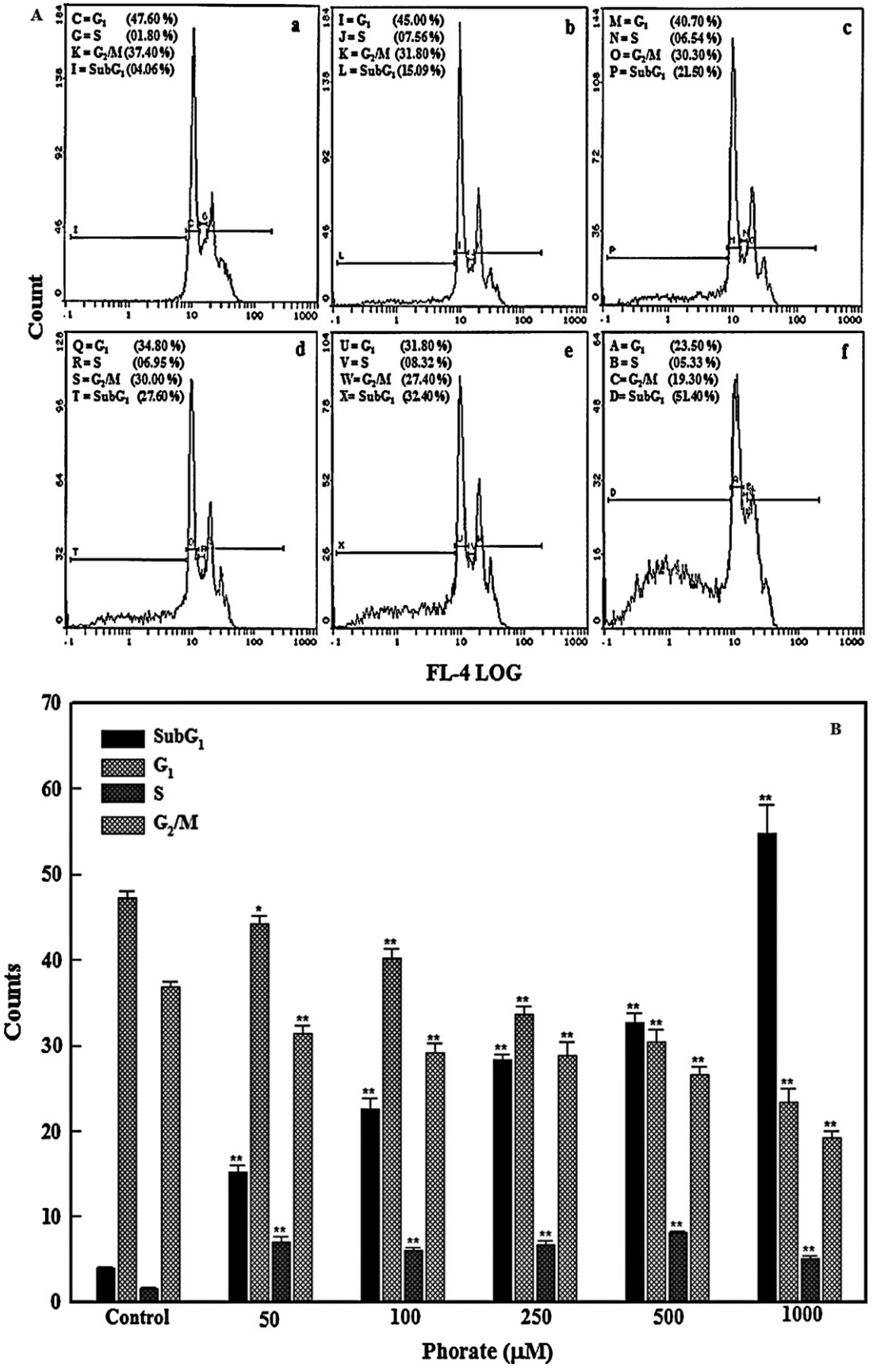


**Fig. 7.** Panel A is a representative flow cytometric image from single experiment exhibiting changes in the progression of normal cell cycle in WISH cells after 72 h of phorate treatment. Sub panels are represented as (a) solvent control (0.1% DMSO); (b) 50 μM; (c) 100 μM; (d) 250 μM; (e) 500 μM and (f) 1000 μM phorate treated WISH cells. Each histogram in panel B represents mean ± S.D. values of different phases of cell cycle obtained from three independent experiments. $^{*}p < 0.05$, $^{**}p < 0.01$ compared to solvent control using one-way ANOVA.

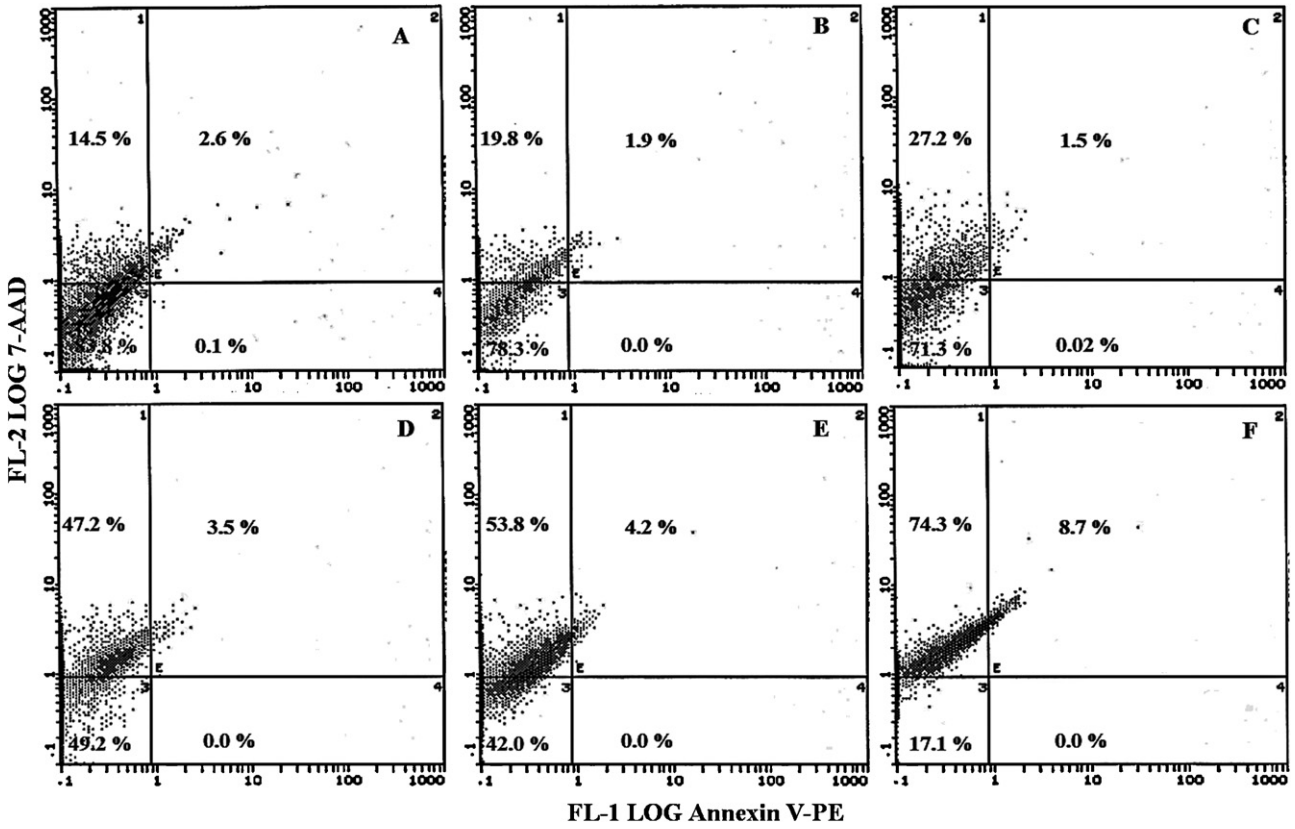


**Fig. 8.** Bivariate flow cytometric analysis of phorate treated WISH cells. Dot plots A–F show the percent distribution of late apoptotic and necrotic cells produced upon 72 h phorate treatment at increasing concentrations. The sub panels depict the annexin V-PE and 7-AAD stained control and phorate treated cells as (A) 0.1% DMSO (as solvent control), (B) 50 μM, (C) 100 μM, (D) 250 μM, (E) 500 μM, (F) 1000 μM phorate.

observed lesser mitochondrial membrane potential ($\Delta\Psi m$) and $G_1$ cell population during cell cycle progression in cells exposed to phorate. The observed shift in Log FL1 peak upon phorate treatment along with the lesser fluorescence, suggests alteration of the inner mitochondrial membrane, and consequent mitochondrial dysfunction. This disruption is most likely due to ROS generation stimulated through metal ions present in cells. Copper is present in the nucleus and its concentration in tissues ranges from 10 to >100 μM [41]. Thus, the spectral changes observed during phorate with ctDNA and Cu (II) ions, and the reduction in $\Delta\Psi m$ demonstrate the significance of phorate–DNA–Cu (II) complexation and its role in intracellular ROS generation. Also, the phorate-treated WISH cells exhibited production of intracellular ROS as indicated by the observed peroxide-dependent oxidation of DCFH-DA to fluorescent 2′,7′-dichlorofluorescin (DCF). Qualitative fluorescence images also revealed the concentration dependent increase in the fluorescence intensity of DCF up to 250 μM phorate in WISH cells.

Furthermore, the appearance of sub-$G_1$ peak with increasing concentration of phorate exposure confirmed the possible involvement of late apoptotic/necrotic pathway, triggered by alteration in mitochondrial and lysosome functions [42,43]. A recent study suggested that mitochondrial events of necrosis involve opening of a pore in the inner mitochondrial membrane, referred as mitochondrial permeability transition pore (MPTP), and loss of $\Delta\Psi m$ [44]. This is consistent with the effects of phorate observed in the MTT assay that suggested mitochondrial dysfunction. Opening of the MPTP results in mitochondrial swelling and rupture of outer mitochondrial membrane during necrosis. This subsequently results in release of apoptogens that likely engage the components of apoptosis machinery to further enhance cell death [44]. Damage to lysosomal membranes is known to release lysosome protease into intracellular spaces, which affects the neighbor cells, and triggers cell death due to necrosis [45]. The flow cytometric analysis of WISH cells using annexin V-PE and 7-ADD staining explicitly demonstrated the phorate induced cell death attributed to late apoptosis and necrosis. Virtually, no annexin $V^+$-PE cells in lower right quadrant appeared at any phorate concentrations in this study, signifies the integrity of plasma membrane and no externalization of phosphatidylserine (PS) due to loss of membrane assembly, which is indicative of early apoptosis [46–48]. However, appearance of significant annexin $V^+$–PE and 7-$ADD^+$ cells population suggests the complete loss of cell membrane integrity in phorate treated WISH cells, eventually causing cell death due to necrosis. In conclusion, the results of the studies presented here are consistent with strong binding affinity of phorate with DNA, preferentially in the minor groove, and demonstrated DNA structural alterations and cellular damage in cultured human cells.

## Conflict of interest

The authors declare that there are no conflicts of interest.

## Acknowledgments

Financial support for this study through Al-Jeraisy Chair for DNA Research, Department of Zoology, College of Science, King Saud University, Riyadh, Saudi Arabia is greatly acknowledged. We are grateful to Dr. Jamal Mustafa, Chemistry Section, University Polytechnic, AMU, Aligarh, India, for his help in elucidating the mechanisms of interactions. Prof. Giesy was supported by the Canada Research Chair program, an at large Chair Professorship at

the Department of Biology and Chemistry and State Key Laboratory in Marine Pollution, City University of Hong Kong, The Einstein Professor Program of the Chinese Academy of Sciences and the Visiting Professor Program of King Saud University.

## Appendix A. Supplementary data

Supplementary data associated with this article can be found, in the online version, at doi:10.1016/j.mrgentox.2012.01.001.

## References

[1] Q. Gan, U. Jans, Nucleophilic reaction of phorate and terbufos with reduced sulfur species under anoxic conditions, J. Agric. Food Chem. 55 (2007) 3546–3554.
[2] S. Vandana, S. Zzaman, Phorate-induced enzymological alterations in mouse olfactory bulb, Brain Res. Bull. 44 (1997) 247–252.
[3] F. Hong, S. Pehkonen, Hydrolysis of phorate using simulated environmental conditions: rates, mechanisms, and product analysis, J. Agric. Food Chem. 46 (1998) 1192–1199.
[4] Y. Wang, R. Du, Simultaneous extraction of trace organophosphorous pesticides from plasma sample by automated solid phase extraction and determination by gas chromatography coupled with pulsed flame photometric detector, Forensic Sci. Int. 198 (2010) 70–73.
[5] S.K. Kashyap, J.P. Jani, H.N. Saiyed, S.K. Gupta, Clinical effects and cholinesterase activity changes in workers exposed to phorate (Thimet), J. Environ. Sci. 19 (1984) 479–489.
[6] G.J. Devine, M.J. Furlong, Insecticide use: contexts and ecological consequences, Agric. Human Values 24 (2007) 281–306.
[7] C.G. Zambonin, M. Quinto, N. DeVietro, F. Palmisano, Solid-phase microextraction gas chromatography mass spectrometry: a fast and simple screening method for the assessment of organophosphorus pesticides residues in wine and fruit juices, Food Chem. 86 (2004) 269–274.
[8] G. Pagliuca, A. Serraino, T. Gazzotti, E. Zironi, A. Borsari, R. Rosmini, Organophosphorus pesticides residues in Italian raw milk, J. Dairy Res. 73 (2006) 1–5.
[9] L. Wang, Y. Liang, X. Jiang, Analysis of eight organophosphorus pesticide residues in fresh vegetables retailed in agricultural product markets of Nanjing China, Bull. Environ. Contam. Toxicol. 81 (2008) 377–382.
[10] S.A. Mansour, M.H. Belal, A.A.K. Abou-Arab, M.F. Gad, Monitoring of pesticides and heavy metals in cucumber fruits produced from different farming systems, Chemosphere 75 (2009) 601–609.
[11] P.C. Abhilash, N. Singh, Pesticide use and application: an Indian scenario, J. Hazard. Mater. 165 (2009) 1–12.
[12] R.C. Sobti, A. Krishnan, C.D. Pffaffenberger, Cytokinetic and cytogenetic effects of some agricultural chemicals on human lymphoid cells in vitro: organophosphates, Mutat. Res. 102 (1982) 89–102.
[13] M.F. Lin, C.L. Wu, T.C. Wang, Pesticide clastogenicity in Chinese hamster ovary cells, Mutat. Res. 188 (1987) 241–250.
[14] A.K. Dhingra, I.S. Grover, N. Adhikari, Chromosomal aberration and micronuclei assays of some systemic pesticides in bone marrow cells, Nucleus 33 (1990) 14–19.
[15] G. Mohanty, J. Mohanty, A.K. Nayak, S. Mohanty, S.K. Dutta, Application of comet assay in the study of DNA damage and recovery in rohu (Labeo rohita) fingerlings after an exposure to phorate, an organophosphate pesticide, Ecotoxicology 20 (2011) 283–292.
[16] M. Dhouib, A. Pfohl-Leszkowicz, G. Dirheimer, A. Lugnier, DNA adducts formation induced in rat by endosulfan, Toxicol. Lett. 78 (1995) 28–29.
[17] A. Laouedj, C. Cschenk, A. Pfohl-leszkowicz, G. Keith, D. Schontz, P. Guillernaut, B. Dether, Detection of DNA adducts in declining hop plants grown on fields formerly treated with heptachlor, a persistent insecticide, Environ. Pollut. 90 (1995) 409–414.
[18] R.G. Shah, J. Lagueux, S. Kapur, P. Levallois, P. Ayotte, M. Tremblay, J. Zee, G.G. Poirier, Determination of genotoxicity of the metabolites of the pesticides guthion, sencor, lorox, reglone, daconil and admire by $^{32}$P-postlabeling, Mol. Cell Biochem. 169 (1997) 177–184.
[19] L.J. Zhang, S.G. Min, G.X. Li, Y.M. Xiong, Y. Sun, The mechanism of carbofuran interacts with calf thymus DNA, Guang Pu. Xue. Yu. Guang. Pu. Fen. Xi. 25 (2005) 739–742.
[20] S. Kashanian, M.B. Gholivand, F. Ahmadi, H. Ravan, Interaction of diazinon with DNA and the protective role of selenium in DNA damage, DNA Cell Biol. 27 (2008) 1–8.
[21] R.C. Gupta, G. Spencer-Beach, Natural and endogenous DNA adducts as detected by $^{32}$P-postlabeling, Regul. Toxicol. Pharmacol. 23 (1996) 14–21.
[22] Q. Saquib, A.A. Al-Khedhairy, S. Al-Arifi, S. Dutta, S. Dasgupta, J. Musarrat, Methyl thiophanate as a DNA minor groove binder produces MT–Cu(II)–DNA ternary complex preferably with AT rich region for initiation of DNA damage, Int. J. Biol. Macromol. 47 (2010) 68–75.
[23] Q. Saquib, A.A. Al-Khedhairy, M.A. Siddiqui, A.S. Roy, S. Dasgupta, J. Musarrat, Preferential binding of insecticide phorate with sub-domain IIA of human serum albumin induces protein damage and its toxicological significance, Food Chem. Toxicol. 49 (2011) 1787–1795.
[24] S.S. Lehrer, G.D. Fasman, The fluorescence of lysozyme and lysozyme substrate complexes, Biochem. Biophys. Res. Commun. 23 (1966) 133–138.
[25] D.M. Chipman, V. Grisaro, N. Sharon, The specificity of binding subsites, J. Biol. Chem. 242 (1967) 4388–4394.
[26] H.M. Berman, J. Westbrook, Z. Feng, G. Gilliland, T.N. Bhat, H. Weissig, I.N. Shindyalov, P.E. Bourne, The Protein Data Bank, Nucleic Acids Res. 28 (2000) 235–242.
[27] G.M. Morris, D.S. Goodsell, R. Huey, A.J. Olson, Distributed automated docking of flexible ligands to proteins: parallel applications of AutoDock 2.4, J. Comput. Aid. Mol. Des. 10 (1996) 293–304.
[28] G.M. Morris, D.S. Goodsell, R.S. Halliday, R. Huey, W.E. Hart, R.K. Belew, A.J. Olson, Automated docking using a lamarckian genetic algorithm and empirical binding free energy function, J. Comput. Chem. 19 (1998) 1639–1662.
[29] W.L. DeLano, The PyMOL Molecular Graphics System, DeLano Scientific, San Carlos, CA, USA, 2004 (last accessed on 21.05.11) http://pymol.sourceforge.net.
[30] M.A. Siddiqui, M.P. Kashyap, V. Kumar, A.A. Al-Khedhairy, J. Musarrat, A.B. Pant, Protective potential of trans-resveratrol against 4-hydroxynonenal induced damage in PC12 cells, Toxicol. In Vitro 24 (2010) 1592–1598.
[31] M.A. Siddiqui, G. Singh, M.P. Kashyap, V.K. Khanna, S. Yadav, D. Chandra, A.B. Pant, Influence of cytotoxic doses of 4-hydroxynonenal on selected neurotransmitter receptors in PC-12 cells, Toxicol. In Vitro 22 (2008) 1681–1688.
[32] Q. Saquib, A.A. Al-Khedhairy, B.R. Singh, J.M. Arif, J. Musarrat, Genotoxic fungicide methyl thiophanate as an oxidative stressor inducing 8-oxo-7,8-dihydro-2′-deoxyguanosine adducts in DNA and mutagenesis, J. Environ. Sci. Health (B) 45 (2010) 1–6.
[33] Z. Darzynkiewicz, S. Bruno, G. Del Bino, Features of apoptosis cells measured by flow cytometry, Cytometry 13 (1992) 795–808.
[34] I. Vermes, C. Haanen, H. Steffens-Nakken, C. Reutelingsperger, A novel assay for apoptosis, flow cytometric detection of phosphatidylserine expression on early apoptotic cells using fluorescein-labeled Annexin V, J. Immunol. Methods 184 (1995) 39–45.
[35] K.S. Ghosh, B.K. Sahoo, D. Jana, S. Dasgupta, Studies on the interaction of copper complexes of (−)-epicatechin gallate and (−)-epigallocatechin gallate with calf thymus DNA, J. Inorg. Biochem. 102 (2008) 1711–1718.
[36] P.D. Ross, S. Subramanian, Thermodynamics of protein association reactions: forces contributing to stability, Biochemistry 20 (1981) 3096–3102.
[37] M.T. Carter, A.J. Bard, Voltammetric studies of the interaction of metal chelates with DNA. 2. Tris-chelated complexes of cobalt (III) and iron (II) with 1,10-phenanthroline and 2,2′-bipyridine, J. Am. Chem. Soc. 111 (1989) 8901–8911.
[38] G.C. Zhao, J.J. Zhang, H.Y. Chen, Voltammetric studies of the interaction of methylene blue with DNA by means of β-cyclodextrin, Anal. Chim. Acta 394 (1999) 337–344.
[39] Q. Saquib, S.M. Attia, M.A. Siddiqui, M. Aboul-Soud, A.A. Al-Khedhairy, J.P. Giesy, J. Musarrat, Phorate-induced oxidative stress, DNA damage and transcriptional activation of p53 and caspases genes in male Wistar rats, Toxicol. Appl. Pharmacol. 259 (2012) 54–65.
[40] P.K. Mahli, I.S. Grover, Genotoxic effects of some organophosphorus pesticides. II. In vivo chromosomal aberration bioassay in bone marrow cells in rat, Mutat. Res. 188 (1987) 45–51.
[41] Q. Saquib, A.A. Al-Khedhairy, S. Al-Arifi, A. Dhawan, J. Musarrat, Assessment of methyl thiophanate–Cu (II) induced DNA damage in human lymphocytes, Toxicol. In Vitro 23 (2009) 848–854.
[42] I. Nicoletti, G. Migliorati, M.C. Pagliacci, F. Grignani, C. Riccardi, A rapid and simple method for measuring thymocyte apoptosis by propidium iodide staining and flow cytometry, J. Immunol. Methods 139 (1991) 271–279.
[43] S. Ravi, K.K. Chiruvella, K. Rajesh, V. Prabhu, S.C. Raghavan, 5-Isopropylidene-3-ethyl rhodanine induce growth inhibition followed by apoptosis in leukemia cells, Eur. J. Med. Chem. 45 (2010) 2748–2752.
[44] R.N. Kitsis, J.D. Molkentin, Apoptotic cell death Nixed by an ER–mitochondrial necrotic pathway, Proc. Natl. Acad. Sci. 107 (2010) 9031–9032.
[45] M. Leist, M. Jäättelä, Four deaths and a funeral: from caspases to alternative mechanisms, Nat. Rev. Mol. Cell Biol. 2 (2001) 589–598.
[46] V.A. Fadok, D.R. Voelker, P.A. Campbell, J.J. Cohen, D.L. Bratton, P.M. Henson, Exposure of phosphatidylserine on the surface of apoptotic lymphocytes triggers specific recognition and removal by macrophages, J. Immunol. 7 (1992) 2207–2216.
[47] S.J. Martin, C.P.M. Reutelingsperger, A.J. McGahon, J. Rader, R.C.A.A. van Schie, D.M. LaFace, D.R. Green, Early redistribution of plasma membrane phosphatidylserine is a general feature of apoptosis regardless of the initiating stimulus. Inhibition by overexpression of Bcl-2 and Abl, J. Exp. Med. 182 (1995) 1545–1557.
[48] C. Diaz, A.J. Schroit, Role of translocases in the generation of phosphatidylserine asymmetry, J. Membr. Biol. 151 (1996) 1–9.